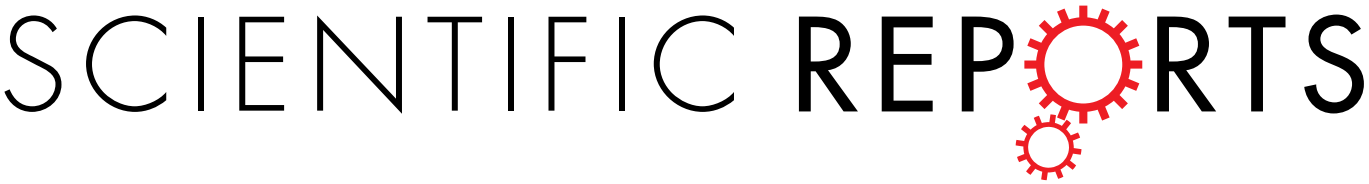

OPEN

Received: 05 September 2016
Accepted: 30 November 2016
Published: 04 January 2017

Strain-Modulated Electronic Structure and Infrared Light Adsorption in Palladium Diselenide Monolayer

Xiaobiao Liu, Hongcai Zhou, Bo Yang, Yuanyuan Qu & Mingwen Zhao

Two-dimensional (2D) transition-metal dichalcogenides (TMDs) exhibit intriguing properties for both fundamental research and potential application in fields ranging from electronic devices to catalysis. Based on first-principles calculations, we proposed a stable form of palladium diselenide ($PdSe_2$) monolayer that can be synthesized by selenizing Pd(111) surface. It has a moderate band gap of about 1.10 eV, a small in-plane stiffness, and electron mobility larger than that of monolayer black phosphorus by more than one order. Additionally, tensile strain can modulate the band gap of $PdSe_2$ monolayer and consequently enhance the infrared light adsorption ability. These interesting properties are quite promising for application in electronic and optoelectronic devices.

Two-dimensional (2D) transition-metal dichalcogenides (TMDs) represent a new family of 2D materials beyond graphene. They have a general formula of MX_2 where M is a transition metal from group 4–10 and X is a chalcogen (S, Se, or Te). In contrast to graphene and their bulk materials, some 2D-TMDs are semiconducting with a sizable band gap, partially due to quantum-confinement effects. So far, theoretical and experimental efforts have been mainly focused on semiconducting 2D-TMDs with M = Mo and W[1–4], due to potential applications in terahertz switch[5], lasers and LEDs[6], ambipolar ionic liquid gated field-effect transistor[7], photo detectors[1], and so on[8]. In a recent work[9], $PtSe_2$ monolayer was synthesized via a single step of direct selenization of a Pt(111) substrate and demonstrated to have potential application as valleytronics and photocatalyst.

Beside platinum, palladium (Pd) can also form binary compounds with Se with different stoichiometries and crystal structures, such as trigonal α-Pd_4Se, tetragonal PdSe, cubic $Pd_{17}Se_{15}$, monoclinic Pd_7Se_2, and orthorhombic $PdSe_2$[10]. Under ambient conditions, $PdSe_2$ crystal appears in an orthorhombic structure with a space group of Pbca similar to the case of PdS_2[11,12]. Using first-principles calculations, Sun *et al.*, proposed a $PdSe_2$ monolayer with semiconducting nature and high Seebeck coefficients[11]. So far, $PdSe_2$ monolayer has not been achieved experimentally, partially due to the strong layer binding energy ~190 meV/atom in orthorhombic $PdSe_2$ bulk crystal which makes the exfoliation of $PdSe_2$ monolayer difficult. However, the recently success in the synthesis of $PtSe_2$ monolayer on Pt(111) substrate via selenization opens an avenue towards this goal.

In this manuscript, we proposed a novel stable configuration of $PdSe_2$ monolayer that can be synthesized by selenizing Pd(111) surface, as shown in Fig. 1(a). Our first-principles calculations indicate that it is energetically comparable to the Pbca phase[11]. Phonon spectrum analysis confirms its dynamics stability. This $PdSe_2$ monolayer has an indirect-band-gap of about 1.10 eV, suitable for application in infrared light region. It also has high electron mobility of about 9800–42000 $cm^2v^{-1}s^{-1}$ which is larger than that in monolayer black phosphorus by more than one order. The in-plane stiffness of 54 J/m^2 is only half of MoS_2, allowing a large tensile strain up to 35%. Additionally, tensile strain can significantly reduce the band gap and consequently enhance the infrared light adsorption ability. These interesting properties are quite promising for application in electronic and optoelectronic devices.

Results and Discussion

Atomic structure and stability. The atomic structure of a freestanding $PdSe_2$ monolayer with a P-3M1 space group is similar with that of $PdSe_2$ monolayer grown on the Pd(111) surface, as shown in Fig. 1(a). Each Pd atom bonds to six Se atoms and each Se atom is coordinated by three Pd atoms. All the Pd atoms are on a same

School of Physics & State Key Laboratory of Crystal Materials, Shandong University, Jinan, Shandong, 250100, China. Correspondence and requests for materials should be addressed to M.W.Z. (email: zmw@sdu.edu.cn)

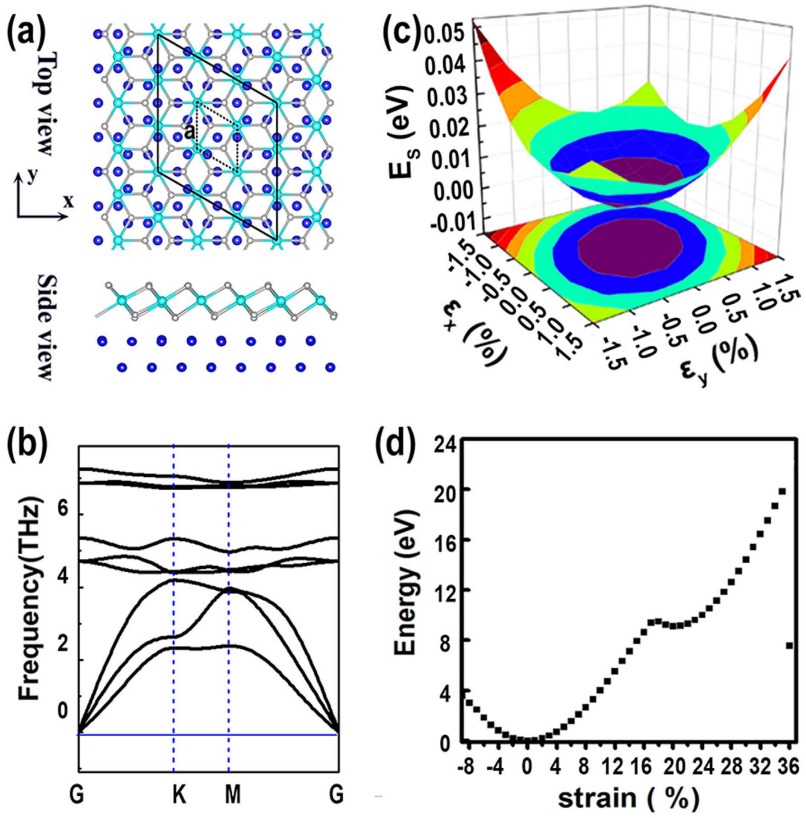

Figure 1. (**a**) The top view and side view of atomic configuration for $PdSe_2$ monolayer on Pd(111) surface. The blue and cyan balls are Pd atoms and gray ball are Se atoms. The small and large black parallelograms represent primitive lattice for monolayer $PdSe_2$ and $PdSe_2$-Pd(111) superstructure, respectively. The black arrows indicate the x- and y-direction for top view. (**b**) The phonon spectrum of $PdSe_2$ monolayer. (**c**) Three-dimensional plot of strain energy E_S (see text) depending on strain of ε_x and ε_y (see text). The color filled contour of the fitted formula is also plotted. (**d**) The energy evolution of $PdSe_2$ monolayer under biaxial compressive and tensile strains. The energy at the equilibrium state was set to zero.

plane sandwiched by two Se planes. The thickness of the freestanding $PdSe_2$ monolayer measured from the distance between the two Se planes is 2.631 Å. The Pd-Se bond length is about 2.528 Å. The optimized lattice constant of the hexagonal lattice is 3.739 Å, quite close to that of the $PtSe_2$ monolayer, 3.7 Å[9]. Notably, a 3×3 $PdSe_2$ monolayer (11.217 Å) matches well with the 4×4 Pd(111) surface (11.186 Å), which implies high plausibility of growing $PdSe_2$ monolayer on Pd(111) surface via selenization. This allows us to build a $PdSe_2$/Pd heterostructure by placing a 3×3 $PdSe_2$ on Pd(111) surface without considering the small lattice mismatch (~0.3%). Compared with freestanding monolayer, the buckling of the supported $PdSe_2$ increases to 2.710 Å and the bond length vary from 2.51 Å to 2.61 Å with an average of 2.55 Å, due to the substrate effect. The distance between $PdSe_2$ monolayer and substrate is about 2.16 Å, and the binding energy between them is −1.04 eV per $PdSe_2$ unit. The $PdSe_2$-Pd(111) interaction is much stronger than the van der Waals (VDW) interaction in graphite (~−36 meV/atom), making the exfoliation of $PdSe_2$ from the Pd substrate difficult.

It is noteworthy that the lattice structure of hexagonal $PtSe_2$ monolayer differs significantly from that cut from orthorhombic $PdSe_2$ crystal[11]. The latter case has orthorhombic symmetry with four-coordinated Pt atoms and two-coordinated Se atoms, and is slightly stable than the hexagonal structure by about 26 meV/atom. However, the hexagonal $PdSe_2$ monolayer matches well with the Pd(111) surface in both symmetry and lattice constant along with a negative binding energy (−1.04 eV per $PdSe_2$ unit) and thus has high plausibility on the Pd(111) surface as the surface is selenized[9].

To confirm the dynamic stability of the $PdSe_2$ monolayer, we calculated the phonon spectrum using a finite displacement method implemented the Phonopy code interfaced the VASP code[13,14]. It was found that the phonon spectrum is free from imaginary frequency modes, as shown in Fig. 1(b), suggesting the dynamic stability of the $PdSe_2$ monolayer. Additionally, there is a small energy gap between the acoustic and optical branches in the phonon spectrum. Such an energy gap can protect the vibration of acoustic modes from being interrupted by optical phonon[15–17], which leads to the resonators with higher quality factor than the graphene resonators[18].

Mechanical properties. Strain is not evitable as a monolayer is grown on a substrate. We therefore investigated the mechanical properties $PdSe_2$ monolayer from first-principles. To obtain the elastic modulus in harmonic range, we employed a rectangular supercell and applied strains along x- and y-direction, as shown in Fig. 1(a). The energy (E_s) dependence of strains is illustrated in Fig. 1(c). The data is fitted to a two-dimensional

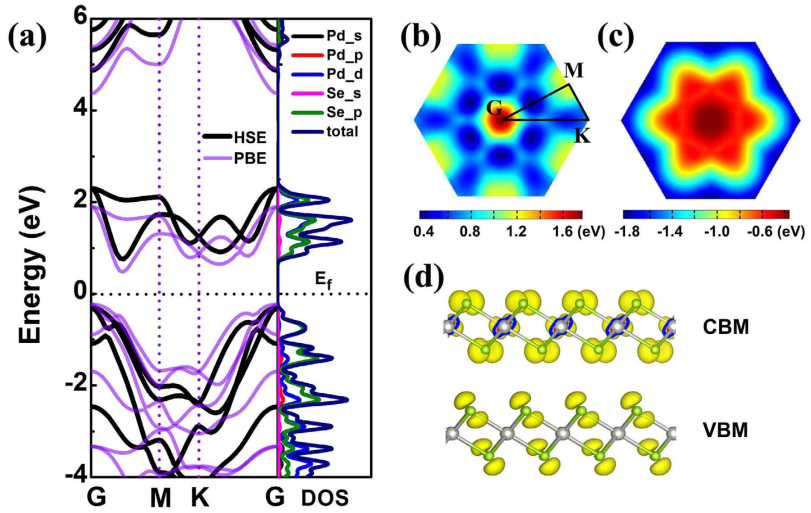

Figure 2. (**a**) Bands structures of $PdSe_2$ monolayer along the high symmetric points in the BZ (right) and orbital-resolved electron density of states (left). The energy at the Fermi level is set to zero. The black lines and purple lines represent the data obtained from HSE and PBE functionals, respectively. M (1/2, 0, 0), G (0, 0, 0) and K (1/3, 1/3, 0) represent high symmetric points in the reciprocal space. The momentum-dependent energy distribution in BZ for (**b**) the lowest unoccupied band and (**c**) the highest occupied band. (**d**) Electron density profiles of the Kohn-Sham wavefunctions for CBM and VBM.

polynomial expressed by $E_s = a_1\varepsilon_x^2 + a_2\varepsilon_y^2 + a_3\varepsilon_x\varepsilon_y$, where ε_x and ε_y represent the strains applied along x- and y-direction, respectively. The total energy of system at the equilibrium state was set to zero. It was found that the two parameters a_1 and a_2 are almost identical due to the isotropy in the honeycomb symmetry[19]. The poisson's ratio (ν) and in-plane stiffness (C) can be obtained as $\upsilon = a_3/a_1$ and $C = 1/A_0((2a_1 - a_3^2)/(2a_1)$[20], where A_0 is the equilibrium area of the structure. The calculated poisson's ratio (0.29) is close to those of MoS_2 (0.25) and silicene (0.30) but larger than that of graphene (0.16). The in-plane stiffness of $PdSe_2$ monolayer, 54 J/m^2, is much smaller than those of MoS_2 (123 J/m^2) and graphene (335 J/m^2)[19,21], suggesting that $PdSe_2$ monolayer is softer than both graphene and MoS_2 monolayer.

The softness of $PdSe_2$ monolayer was also confirmed by the energetic and structural evolution as a function of biaxial strain. Figure 1(d) gives the energy increase of $PdSe_2$ monolayer as the biaxial strain varies from −9% (compression) up to 35%. It is interesting to see that energy varies continuously without abrupt decrease, indicating that no Pd-Se bonds are broken in this region. As the tensile strain exceeds 35%, energy decreases drastically and irreversible structure modification along with Pd-Se bond breakage takes place. The two energy local minima at $\varepsilon = 0$ and 20.4% correspond to the equilibrium state and a metal-stable state of $PdSe_2$ monolayer. The later configuration has the Pd-Se bond length of 2.639 Å, slightly longer than that of the equilibrium state by about 4.4%, but the thickness is greatly reduced to 0.918 Å compared to the equilibrium state value 2.631 Å. The metastable state represents a low-buckled configuration of $PdSe_2$ monolayer under high tensile strain. Similar results have also been reported for silicene, but the critical tensile strain in $PdSe_2$ monolayer is much larger than that in silicene[21].

Electronic properties. We then calculated the electronic structure of $PdSe_2$ monolayer from first-principles. We employed the PBE functional and Heyd–Scuseria–Ernzerhof (HSE) screened Coulomb hybrid density functional[22] in the framework of DFT. The band structure and electronic density of states (DOS) near the Fermi level are illustrated in Fig. 2(a). Both functionals gave the semiconducting nature of $PdSe_2$ monolayer with an indirect band gap, similar to the case of orthorhombic $PdSe_2$[11]. The valence band maximum (VBM) resides at the Γ (0, 0, 0) point while the conduction band minimum (CBM) locates in between Γ (0, 0, 0) and M (0.5, 0, 0). Six valleys are therefore found in the whole Brillouin zone as shown in Fig. 2(b), which gives opportunities to valley devices. The PBE functional underestimated the band gap value (0.7 eV) compared with HSE functional (1.10 eV). The band gap of $PdSe_2$ monolayer is slightly smaller than that of $PtSe_2$ monolayer (1.2 eV)[9] and orthorhombic $PdSe_2$(1.43 eV)[11] and suitable for adsorbing infrared light. From the orbital-resolved electron density of states shown in Fig. 2(a), we can see that the VBM is mainly contributed by the 4p orbits of Se atoms, while the CBM comes mainly from the 4d orbits of Pd and 4p orbits of Se. This is consistent with the features of the Kohn-Sham wavefunctions of the VBM and CBM plotted in Fig. 2(d). Considering Pd is a heave element, we also took the spin-orbit coupling (SOC) effect into account in electronic structure calculations. It was found that the energy degeneracy at some highly-symmetric points in BZ is lifted due to SOC (Fig. S2 in Supplementary Information). Both the valence and conduction bands are shifted downward and the global indirect band gap is decreased by about 0.2 eV. The reduced band gap would lead to red shift of optical adsorption peaks and thus facilitate the adsorption of infrared light.

When $PdSe_2$ monolayer is grown on Pd(111) substrate, the energy bands of semiconducting $PdSe_2$ and metallic Pd substrate mix together. Slight electron redistribution takes place in $PdSe_2$ monolayer. About 0.05 electrons

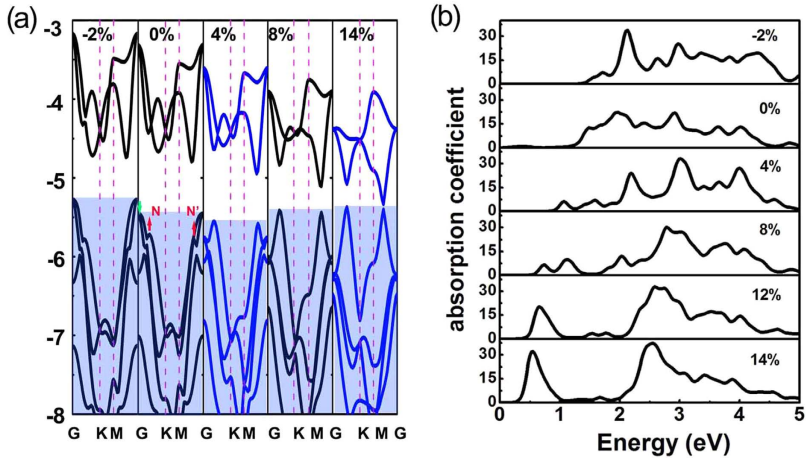

Figure 3. (**a**) The electronic band structures of $PdSe_2$ monolayer under different strains obtained from PBE functional. The vacuum level is set to 0 eV. The regions of valence bands are covered by translucent blue. (**b**) Strain-dependent absorption coefficient of $PdSe_2$ monolayer calculated by using HSE functional. The insert number donates the biaxial strain.

per Se atom transfer from upper Se layer to down Se layer, while the electron transfer from $PdSe_2$ monolayer to substrate is almost negligible (~0.007 |e| per $PdSe_2$ unit). This slightly reduces the workfunction of $PdSe_2$ to 5.20 eV compared with that of freestanding $PdSe_2$ monolayer (5.40 eV). We also calculated the electronic structures of $PdSe_2$ multilayers built by stacking $PdSe_2$ monolayers with different patterns. For the $PdSe_2$ bilayer, AA stacking pattern is energetically more favorable than AB pattern (Supplementary Information). The interlayer interaction greatly reduces the band gap of 2D $PdSe_2$. The band gap of the $PdSe_2$ bilayer with AB pattern is only 0.33 eV (PBE), while the energetically preferred AA pattern becomes metallic.

We also calculated the electron mobility of $PdSe_2$ monolayer using the phonon-limited scattering model[23,24]. In the method, the electron mobility can be evaluated using the expression[24–26], $\mu_e = e\hbar C_{2D}/(k_B T m_e m_a (E_l)^2)$; where e is the electron charge, $\hbar$ is Planck's constant divided by 2π, k_B is Boltzmann's constant and T is the temperature. m_e is effective mass of electron in the transport direction (either m_x or m_y along the x and y direction, respectively) and m_a is the averaged effective mass of that along x and y direction determined by $m_a = \sqrt{m_x^* m_y^*}$. Deformation potential constant of CBM (E_l) for electrons along the transport direction is defined by $E_l = \Delta V/(\Delta l/l_0)$, ΔV is the energy change of CBM, l_0 is the lattice constant in the transport direction and Δl is the change of l_0. The elastic modulus C_{2D} of the longitudinal strain in the propagation directions of the longitudinal acoustic wave is derived from $(E - E_0)/S_0 = C(\Delta l/l_0)^2/2$; where E is the total energy and S_0 is the lattice area at equilibrium for 2D system. The electron mobilities along x- and y-direction are 9800 $cm^2v^{-1}s^{-1}$ and 42000 $cm^2v^{-1}s^{-1}$ at 300 K, respectively. These values are much higher than that in monolayer black phosphorus by more than one order of magnitudes. Such high electron mobility is quite promising for improving the photocatalytic activity of $PdSe_2$ monolayer, because the photo-generated electrons can be easily transferred[9].

The electronic structure modification of $PdSe_2$ monolayer in response to tensile strain was then investigated. With the increase of tensile strain, the band gap of $PdSe_2$ monolayer decreases and comes to close as the tensile is larger than 14%. More interestingly, compressive strain also reduces the band gap of $PdSe_2$ monolayer. To reveal the origins of the strain-induced band gap modulation, we plotted the band structures of $PdSe_2$ monolayer under difference strains in Fig. 3(a). From this figure, we can see that under a tensile strain, the CBM move downwards while the VBM varies slightly, reducing the band gap. This may be related to the enhancement of the Se_4p and Pd_4d interaction due to the shorten distance between the Se plane and Pd plane. Under a compressive strain, however, the VBM is sensitive to strain and shifts upwards, leading to band gap reduction. Besides, it is interesting to see that tensile strain decreases the energy of the G points (illustrated by green arrow in Fig. 3(a)), and lifts the energies of the N and N' points (illustrated by red arrow in Fig. 3(a)). As the tensile strain is larger than 4%, the energy difference between the N and N' points becomes very small, making the $PdSe_2$ a quasi-direct band semiconductor.

Optical adsorption. The strain-induced band gap reduction affects the optoelectronic properties of $PdSe_2$ monolayer. We calculated the imaginary part of complex dielectric function using the expression:

$$\epsilon''_{\alpha\beta(\omega)} = \frac{4\pi^2 e^2}{\Omega} \times \lim_{q\to 0} \frac{1}{q^2} \sum_{c,v,k} 2\omega_k \delta(\varepsilon_{ck} - \varepsilon_{vk} - \omega) \times < \mu_{ck+eq} \left| \mu_{vk} \right| > < \mu_{ck+eq} \left| \mu_{vk} \right| >^* .$$

The indices c and v refer to conduction and valence band states respectively. u_{ck} is the cell periodic part of the orbitals at the k-point $\mathbf{k}$. ω is the frequency of the incident photon. The real part of the dielectric function $\epsilon'_{\alpha\beta(\omega)}$ is obtained from the imaginary part with the Kramers-Kroning relations. The optical absorption coefficient is given

by $I(\omega) = \sqrt{2}\omega[\sqrt{\epsilon'(\omega)^2 + \epsilon''(\omega)^2} - \epsilon'(\omega)]^{\frac{1}{2}}$; where ϵ' and ϵ'' is the real and imaginary part of complex dielectric function. The optical absorption coefficient I(ω) calculated using HSE functional is plotted in Fig. 3(b). At equilibrium state, the adsorption peaks locate in the visible light and ultraviolet light region. A small compression has little affect on the adsorption properties. When a tensile strain is applied to $PdSe_2$ monolayer, adsorption peaks come to appear in the low energy region, due to the band gap reduction. Meanwhile, the adsorption to visible light is partially screened. For example, under the tensile strains larger than 12%, the adsorption coefficients are almost zero in the energy region from 1.0–2.0 eV. These fascinating properties are quite promising for infrared detectors where the screening of visible light adsorption is needed.

Conclusion

In summary, based on first-principles calculations, we proposed a stable form of palladium diselenide ($PdSe_2$) monolayer that may be synthesized by selenizing Pd(111) surface. The $PdSe_2$ monolayer possesses a moderate band gap of about 1.10 eV and high electron motilities of about 9800–42000 $cm^2v^{-1}s^{-1}$, suitable for the electronic and optoelectronic devices working at infrared light region. The band gap of $PdSe_2$ monolayer can be modulated by applying tensile strains. With the increase of tensile strain, the band gap decreases and comes to close as the tensile strain is larger than 14%. Consequently, the light adsorption ability of the $PdSe_2$ monolayer in infrared light region is greatly enhanced. These findings are quite promising for application in electronic and optoelectronic devices.

Methods

Our first-principles calculations were performed within density-functional theory (DFT) using the Vienna ab initio simulation package known as the VASP code[27–29]. The projector augmented wave method (PAW)[30,31] was used to describe the electronic-ion interaction. The energy cutoff of the plane waves was set to 450 eV with an energy precision of 10^{-5} eV. The electron exchange–correlation function was treated using a generalized gradient approximation (GGA) in the form proposed by Perdew, Burke, and Ernzerhof (PBE)[32]. The Monkhorst-Pack *k*-point meshes[33] for the Brillouin zone (BZ) sampling used in structural optimization and electronic structure calculations are $8 \times 8 \times 1$ and $15 \times 15 \times 1$, respectively. The primitive cell contains one Pd atom and two Se atoms which is periodically repeated along the x- and y-directions. A vacuum region up to 15 Å was applied along the z-direction to exclude the interaction between adjacent images. Both atomic positions and lattice vectors were fully optimized using the conjugate gradient (CG) algorithm until the maximum atomic forces were less than 0.0005 eV/Å. The lattice constants of the orthorhombic $PdSe_2$ crystal (a = 5.752 Å, b = 5.926 Å) obtained from our calculations agree well with the experimental data (a = 5.746 Å, b = 5.868 Å)[12], confirming the validity of this strategy.

References

1. Lan, C., Li, C., Yin, Y. & Liu, Y. Large-area synthesis of monolayer WS_2 and its ambient-sensitive photo-detecting performance. *Nanoscale* **7,** 5974–5980 (2015).
2. McCreary, K. M., Hanbicki, A. T., Jernigan, G. G., Culbertson, J. C. & Jonker, B. T. Synthesis of Large-Area WS_2 monolayers with Exceptional Photoluminescence. *Sci. Rep*. **6,** 19159 (2016).
3. Mitioglu, A. A. *et al.* Magnetoexcitons in large area CVD-grown monolayer MoS_2 and $MoSe_2$ on sapphire. *Phys. Rev. B* **93,** 165412 (2016).
4. Xu, Z. Q. *et al.* Synthesis and Transfer of Large-Area Monolayer WS_2 Crystals: Moving Toward the Recyclable Use of Sapphire Substrates. *ACS Nano* **9,** 6178–6187 (2015).
5. Cao, Y. *et al.* Optically tuned terahertz modulator based on annealed multilayer MoS_2. *Sci. Rep*. **6,** 22899 (2016).
6. Hu, P. *et al.* Control of Radiative Exciton Recombination by Charge Transfer Induced Surface Dipoles in MoS_2 and WS_2 Monolayers. *Sci. Rep.* **6,** 24105 (2016).
7. Jo, S., Ubrig, N., Berger, H., Kuzmenko, A. B. & Morpurgo, A. F. Mono- and bilayer WS_2 light-emitting transistors. *Nano Lett.* **14,** 2019–2025 (2014).
8. Cao, T. *et al.* Valley-selective circular dichroism of monolayer molybdenum disulphide. *Nat. Commun.* **3,** 887 (2012).
9. Wang, Y. *et al.* Monolayer $PtSe_2$, a New Semiconducting Transition-Metal-Dichalcogenide, Epitaxially Grown by Direct Selenization of Pt. *Nano Lett.* **15,** 4013–4018 (2015).
10. Bordier, S., Chocard, A. & Gossé, S. Thermodynamic assessment of the palladium–selenium (Pd–Se) system. *J. Nucl. Mater.* **451,** 120–129 (2014).
11. Sun, J., Shi, H., Siegrist, T. & Singh, D. J. Electronic, transport, and optical properties of bulk and mono-layer $PdSe_2$. *Appl. Phys. Lett.* **107,** 153902 (2015).
12. Soulard, C. *et al.* Experimental and Theoretical Investigation on the Relative Stability of the PdS_2- and Pyrite-ype Structures of $PdSe_2$. *Inorg. Chem.* **43,** 1943–1949 (2004).
13. Alfè, D. PHON: A program to calculate phonons using the small displacement method. *Comput. Phys. Commu*. **180,** 2622–2633 (2009).
14. K. Parlinski, Z. Q. L. & Kawazoe, Y. First-Principles Determination of the Soft Mode in Cubic ZrO_2. *Phys. Rev. Lett.* **78,** 4063–4066 (1997).
15. Jiang, J. W. Phonon bandgap engineering of strained monolayer MoS_2. *Nanoscale* **6,** 8326–8333 (2014).
16. Molina-Sánchez, A. & Wirtz, L. Phonons in single-layer and few-layer MoS_2 and WS_2. *Phys. Rev. B* **84,** 155413 (2011).
17. Sengupta, A., Chanana, A. & Mahapatra, S. Phonon scattering limited performance of monolayer MoS2 and WSe2 n-MOSFET. *AIP Adv*. **5,** 027101 (2015).
18. Jiang, J. W., Park, H. S. & Rabczuk, T. MoS_2 nanoresonators: intrinsically better than graphene? *Nanoscale* **6,** 3618–3625 (2014).
19. Yue, Q. *et al.* Mechanical and electronic properties of monolayer MoS_2 under elastic strain. *Phys. Rev. A* **376,** 1166–1170 (2012).
20. Qin, R., Wang, C.-H., Zhu, W. & Zhang, Y. First-principles calculations of mechanical and electronic properties of silicene under strain. *AIP Adv.* **2,** 022159 (2012).
21. Şahin, H. *et al.* Monolayer honeycomb structures of group-IV elements and III-V binary compounds: First-principles calculations. *Phys. Rev. B* **80,** 155453 (2009).
22. Heyd, J., Scuseria, G. E. & Ernzerhof, M. Hybrid functionals based on a screened Coulomb potential. *J. Chem. Phys.* **118,** 8207–8215 (2003).

23. Xi, J., Long, M., Tang, L., Wang, D. & Shuai, Z. First-principles prediction of charge mobility in carbon and organic nanomaterials. *Nanoscale* **4,** 4348–4369 (2012).
24. Bruzzone, S. & Fiori, G. Ab-initio simulations of deformation potentials and electron mobility in chemically modified graphene and two-dimensional hexagonal boron-nitride. *Appl. Phys. Lett.* **99,** 222108 (2011).
25. Qiao, J., Kong, X., Hu, Z. X., Yang, F. & Ji, W. High-mobility transport anisotropy and linear dichroism in few-layer black phosphorus. *Nat. Commun.* **5,** 4475 (2014).
26. Xie, J., Zhang, Z. Y., Yang, D. Z., Xue, D. S. & Si, M. S. Theoretical Prediction of Carrier Mobility in Few-Layer BC_2N. *The Tournal of Physical Chemistry Letters* **5,** 4073–4077 (2014).
27. Kress, G. & Furthmuller, J. Efficiency of ab-initio total energy calculations for metals and semiconductors using a plane-wave basis set. *Comput. Mater. Sci.* **6,** 15 (1996).
28. Kresse, G. & Hafner, J. Ab initio molecular dynamics for liquid metals. *Phys. Rev. B* **47,** 558–561 (1993).
29. Kresse, G. & Hafner, J. Ab initio molecular dynamics for open-shell transition metals. *Phys. Rev. B* **48,** 13115–13118 (1993).
30. Kresse, G. & Furthmuller, J. Efficient iterative schemes for ab initio total-energy calculations using a plane-wave basis set. *Phys. Rev. B* **54,** 11169–11186 (1996).
31. Kresse, G. & Joubert, D. From ultrasoft pseudopotentials to the projector augmented-wave method. *Phys. Rev. B* **59,** 1758–1775 (1999).
32. Perdew, J. P., Burke, K. & Ernzerhof, M. Generalized gradient approximation made simple. *Phys. Rev. Lett.* **77,** 3865–3868 (1996).
33. Monkhorst, H. J. & Pack, J. D. Special points for Brillouin-zone integrations. *Phys. Rev. B* **13,** 5188–5192 (1976).

Acknowledgements

This work is supported by the National Key Research and Development Program of China grant 2016YFA0301204, the National Natural Science Foundation of China (No. 21433006), the 111 project (No. B13029) and the National Super Computing Centre in Jinan.

Author Contributions

X.L. performed the calculations of optical and electronic parts, analyzed the data and drafted the manuscript. C.H., B.Y. and Y.Q. contributed to the calculations of mechanism properties. M.Z. conceived the study and revised the manuscript. All authors read and approved the final manuscript.

Additional Information

Supplementary information accompanies this paper at http://www.nature.com/srep

Competing financial interests: The authors declare no competing financial interests.

How to cite this article: Liu, X. *et al.* Strain-Modulated Electronic Structure and Infrared Light Adsorption in Palladium Diselenide Monolayer. *Sci. Rep.* **7**, 39995; doi: 10.1038/srep39995 (2017).

Publisher's note: Springer Nature remains neutral with regard to jurisdictional claims in published maps and institutional affiliations.